JACS
JOURNAL OF THE AMERICAN CHEMICAL SOCIETY

Subscriber access provided by American Chemical Society

Article

Inhibition and Aerobic Inactivation Kinetics of *Desulfovibrio fructosovorans* NiFe Hydrogenase Studied by Protein Film Voltammetry

Christophe Lger, Sbastien Dementin, Patrick Bertrand, Marc Rousset, and Bruno Guigliarelli

J. Am. Chem. Soc., **2004**, 126 (38), 12162-12172• DOI: 10.1021/ja046548d • Publication Date (Web): 02 September 2004

Downloaded from http://pubs.acs.org on April 1, 2009

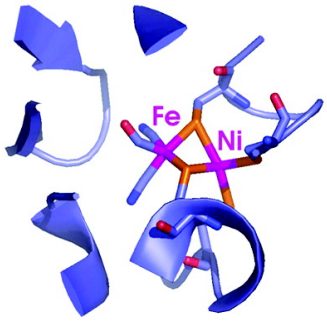

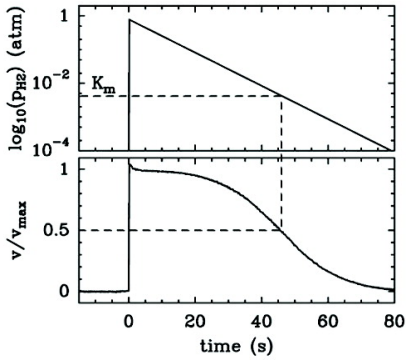

More About This Article

Additional resources and features associated with this article are available within the HTML version:

- Supporting Information
- Links to the 10 articles that cite this article, as of the time of this article download
- Access to high resolution figures
- Links to articles and content related to this article
- Copyright permission to reproduce figures and/or text from this article

View the Full Text HTML

ACS Publications
High quality. High impact.

Journal of the American Chemical Society is published by the American Chemical Society. 1155 Sixteenth Street N.W., Washington, DC 20036

J|A|C|S
ARTICLES
Published on Web 09/02/2004

Inhibition and Aerobic Inactivation Kinetics of *Desulfovibrio fructosovorans* NiFe Hydrogenase Studied by Protein Film Voltammetry

Christophe Léger,* Sébastien Dementin, Patrick Bertrand, Marc Rousset, and Bruno Guigliarelli

Contribution from the Unité de Bioénergétique et Ingénierie des Protéines, Institut de Biologie Structurale et Microbiologie, CNRS UPR9036 et Université de Provence, 31, chemin Joseph Aiguier, 13402, Marseille, France

Received June 11, 2004; E-mail: christophe.leger@ibsm.cnrs-mrs.fr

Abstract: We have used protein film voltammetry to study the NiFe hydrogenase from *Desulfovibrio fructosovorans*. We show how measurements of transient activity following the addition in the electrochemical cell of H_2, CO, or O_2 allow simple and virtually instantaneous determinations of the Michaelis constant, inhibition constant, or rate of inactivation, respectively, thus opening new opportunities to study the active site of NiFe hydrogenases. The binding and release of CO occur within a fraction of a second, and we determine and discuss how its affinity for the active site changes as the driving force for the H^+/H_2 reaction is continuously varied. Inactivation by O_2 is a slow, bimolecular process (with pH-independent rate constant $\approx 3 \times 10^4$ s^{-1} M^{-1} at 40 °C, under one atm of H_2) that leads to a mixture of fully oxidized states, and unlike the case of CO inhibition, the active site is not fully protected by H_2. This experimental approach could be used to study the reaction of other multicentered metalloenzymes with their gaseous substrates or inhibitors.

Introduction

While reserves of fossil fuels are shrinking and concern is growing about our overheating world, hydrogen is emerging as an alternative energy carrier, which may eventually help to solve the energy and environmental crises. However, the synthesis of cheap catalysts for H_2 oxidation and formation is a prerequisite for generalized use of fuel cells. In this context, it is striking that most living organisms,[1] and indeed 99% of bacteria, are able to use H_2 as an energy source and that the active site of hydrogenases,[2,3] the enzymes which catalyze the biological conversion between H^+ and H_2, is a cluster containing common metals: iron and nickel.

Hydrogenases (hases) are classified on the basis of their metal content. Iron-only hases are bidirectional enzymes, usually involved in H_2 evolution, whereas NiFe hases are often used as electron donors to anaerobic respiratory chains and are thought of as being H_2 uptake catalysts. Several NiFe hydrogenases, including that from the sulfate reducing bacterium *Desulfovibrio fructosovorans* (Df),[4,5] have been crystallized. These enzymes, the molecular weight of which is about 90 kDa, contain a deeply buried $NiFe(CN)_2CO$ binuclear active site in which the metal ions are bound to the protein by four cysteinyl thiolates. Dihydrogen diffuses along conserved, mainly hydrophobic channels[5] and binds to the active site where it is heterolytically cleaved;[6−8] the electrons are then transferred to the physiological redox partner via a linear chain of iron−sulfur clusters,[4] and a conserved glutamate in the active site is the first proton acceptor.[9] This occurs with a turnover as high as several thousands per second.[12]

The NiFe active site has been characterized in a number of distinct redox states (for review, see refs 2 and 3). The active, oxidized form that binds H_2 is called Ni−SI. In this EPR-silent state, the metal ions are Ni(II) and Fe(II). The one-electron reduction of Ni−SI leads to an EPR-active state called Ni−C, where a hydride bridges the Ni(III) and Fe(II) ions.[19−22] The

(1) Vignais, P. M.; Billoud, B.; Meyer, J. *FEMS Microbiol. Rev.* **2001**, *25*, 455−501.
(2) Cammack, R.; Frey, M.; Robson, R., Eds. *Hydrogen as a fuel, learning from Nature*; Taylor and Francis: London and New York, 2001.
(3) Armstong, F. A. *Curr. Opin. Chem. Biol.* **2004**, *8*, 133−140.
(4) Rousset, M.; Montet, Y.; Guigliarelli, B.; Forget, N.; Asso, M.; Bertrand, P.; Fontecilla-Camps, J. C.; Hatchikian, E. C. *Proc. Natl. Acad. Sci. U.S.A.* **1998**, *95*, 11625−11630.
(5) Volveda, A.; Montet, Y.; Vernede, X.; Hatchikian, E. C.; Fontecilla-Camps, J. C. *Int. J. Hydrogen Energy* **2002**, *27*, 1449−1461.
(6) Maroney, M. J.; Bryngelson, P. A. *J. Biol. Inorg. Chem.* **2001**, *6*, 453−459.
(7) Siegbahn, P. E. M.; Blomberg, M. R. A.; Wirstam, M.; Crabtree, R. H. *J. Biol. Inorg. Chem.* **2001**, *6*, 460−466.
(8) Fan, H.-J.; Hall, M. B. *J. Biol. Inorg. Chem.* **2001**, *6*, 467−473.
(9) Dementin, S.; Burlat, B.; De Lacey, A. L.; Pardo, A.; Adryanczyk-Perrier, G.; Guigliarelli, B.; Fernandez, V. M.; Rousset, M. *J. Biol. Chem.* **2004**, *279*, 10508−10513.
(10) Armstrong, F. A.; Heering, H. A.; Hirst, J. *Chem. Soc. Rev.* **1997**, *26*, 169−179.
(11) Léger, C.; Elliott, S. J.; Hoke, K. R.; Jeuken, L. J. C.; Jones, A. K.; Armstrong, F. A. *Biochemistry* **2003**, *42*, 8653−8662.
(12) Pershad, H. R.; Duff, J. L. C.; Heering, H. A.; Duin, E. C.; Albracht, S. P. J.; Armstrong, F. A. *Biochemistry* **1999**, *38*, 8992−8999.
(13) Léger, C.; Jones, A. K.; Roseboom, W.; Albracht, S. P. J.; Armstrong, F. A. *Biochemistry* **2002**, *41*, 15736−15746.
(14) Léger, C.; Jones, A. K.; Albracht, S. P. J.; Armstrong, F. A. *J. Phys. Chem. B* **2002**, *106*, 13058−13063.
(15) Jones, A. K.; Lamle, S. E.; Pershad, H. R.; Vincent, K. A.; Albracht, S. P. J.; Armstrong, F. A. *J. Am. Chem. Soc.* **2003**, *125*, 8505−8514.
(16) Lamle, S. E.; Vincent, K. A.; Halliwell, L. M.; Albracht, S. P. J.; Armstrong, F. A. *J. Chem. Soc., Dalton Trans.* **2003**, 4152−4157.
(17) Jones, A. K.; Sillery, E.; Albracht, S. P. J.; Armstrong, F. A. *Chem. Commun.* **2002**, 866−867.

10.1021/ja046548d CCC: $27.50 **© 2004 American Chemical Society**

EPR-silent Ni(II)Fe(II) Ni−R state, catalytically competent to evolve H_2, is obtained upon further reduction (see Scheme S3 in the Supporting Information). All these species have distinct, pH-dependent FTIR signatures due to the absorption bands of the intrinsic CO and CN ligands.[23,24]

The Ni−SI form can be further oxidized to one of two inactive states called Ni−A and Ni−B (sometimes called "Ni_u^*" and "Ni_r^*", respectively), in which the Ni and the Fe are bridged by an oxygenated species[25] that is absent in the structure of the reduced, active protein. Ni−B can be formed upon aeration at high pH or under anaerobic, oxidizing conditions and is easily reduced and reactivated; the formation of Ni−A requires O_2, and its reduction under H_2 at ambient temperature takes hours.[15,26−30] The structural difference between the inactive states remains a matter of debate.[29,31−33] Contrarily to O_2, exogenous CO binds reversibly to the active site Ni.[16,34−40] It inhibits both H_2 evolution and uptake and competes with H_2.[41−43]

The steady-state activity of hydrogenases can be quantified in a number of different ways that each probe the global rate of a specific sequence of chemical events. (i) The ortho-H_2/para-H_2 conversion, which only requires that H_2 is reversibly split at the active site, is detected by the change in thermal conductivity;[44] (ii) the H/D exchange, which relates to hydrogen activation and proton transfers, is measured by mass spectrometry; (iii) H_2 consumption or production is coupled to the change in redox state of artificial or physiological redox partners, and spectrophotometry is used to monitor the rate of the overall process, which involves H_2 diffusion and splitting, intramolecular electron and proton transfers, and intermolecular electron transfer. Fraser Armstrong and co-workers, in Oxford, introduced recently protein film voltammetry (PFV)[10,11] as an alternative technique to study the H^+/H_2 conversion in either direction.[11−18]

Using PFV, the redox enzyme is adsorbed onto an electrode, and electron transfer to and from the protein is direct (i.e., not mediated by soluble redox dyes). The redox state of the enzyme depends on the electrode potential, and the catalytic current is simply proportional to the enzyme's activity. Recent PFV studies of *Allochromatium vinosum* (Av) hase have given a wealth of diverse and original information about the redox properties of the catalytic intermediates, including coupled chemical equilibria such as protonation,[13] the anaerobic, oxidative inactivation of the active site,[15] interfacial electron-transfer kinetics,[14] reaction with O_2 and kinetic isotope effects.[16] The spectacular result which initiated this series of investigations is that the activity of Av-hase adsorbed on an electrode is at least an order of magnitude greater than that measured in solution assays;[12] this shows that the oxidation of the enzyme by the soluble dyes limits turnover in conventional experiments and makes PFV an indispensable tool to probe the catalytic efficiency of the NiFe active site.

An advantage of PFV with respect to solution assays is that in cyclic voltammetry experiments, the driving force for the catalytic process can be continuously varied by sweeping the electrode potential (slowly enough that kinetics remains at steady-state) while the magnitude of the catalytic current informs on the accumulation, under given redox conditions, of the state competent for catalysis. Alternatively, to deconvolve the contributions of time and potential, it can be more informative to step the electrode potential; then, the current (or change in current against time) reflects the rate (or change in rate) of the catalytic process.[45] This transient-state approach was used recently to investigate the kinetics of formation of Ni−B in Av-hase.[15]

In this paper, we take this option further, and we show how measurements of activity against time, while the concentration of H_2, CO, or O_2 is slowly changing, allow the characterization of the kinetics of binding and inactivation in a very original and time-saving manner. This provides us with a new strategy to characterize the sensibility of NiFe hydrogenases to inhibitors.

Materials and Methods

Samples of WT *D. fructosovorans* NiFe hydrogenase were prepared as described in ref 9.

Protein film voltammetry experiments were performed with solutions containing mixed buffers consisting of MES, HEPES, sodium acetate, TAPS, and CHES (5 mM of each component), 1 mM EDTA, and 0.1 M NaCl as supporting electrolyte. Mixtures were titrated with NaOH or HCl to the desired pH.

(18) Butt, J. N.; Filipiak, M.; Hagen, W. R. *Eur. J. Biochem.* **1997**, *245*, 116−122.
(19) Dole, F.; Fournel, A.; Magro, V.; Hatchikian, E. C.; Bertrand, P.; Guigliarelli, B. *Biochemistry* **1997**, *36*, 7847−7854.
(20) DeGioia, L.; Fantucci, P.; Guigliarelli, B.; Bertrand, P. *Inorg. Chem.* **1999**, *38*, 2658−2662.
(21) Foester, S.; Stein, M.; Brecht, M.; Ogata, H.; Higuchi, Y.; Lubitz, W. *J. Am. Chem. Soc.* **2002**, *125*, 83−93.
(22) Brecht, M.; vanGastel, M.; Buhrke, T.; Friedrich, B.; Lubitz, W. *J. Am. Chem. Soc.* **2003**, *125*, 13075−13083.
(23) Happe, R. P.; Roseboom, W.; Pierik, A. J.; Albracht, S. P. J.; Bagley, K. A. *Nature* **1997**, *385*, 126−126.
(24) De Lacey, A. L.; Hatchikian, E. C.; Volbeda, A.; Frey, M.; Fontecilla-Camps, J. C.; Fernandez, V. M. *J. Am. Chem. Soc.* **1997**, *119*, 7181−7189.
(25) Carepo, M.; Tiermey, D. L.; Brondino, C. D.; Yang, T. C.; Pamplona, A.; Telser, J.; Moura, I.; Moura, J. J. G.; Hoffman, B. M. *J. Am. Chem. Soc.* **2001**, *124*, 281−286.
(26) Fernandez, V. M.; Hatchikian, E. C.; Cammack, R. *Biochim. Biophys. Acta* **1985**, *832*, 69−79.
(27) Hallahan, D. L.; Fernandez, V. M.; Hall, D. O. *Eur. J. Biochem.* **1987**, *165*, 621−625.
(28) Albracht, S. P. J. *Biochim. Biophys. Acta* **1994**, *1188*, 167−204.
(29) Bleijlevens, B.; Faber, B. W.; Albracht, S. P. J. *J. Biol. Inorg. Chem.* **2001**, *6*, 763−769.
(30) Kurkin, S.; George, S. J.; Thorneley, R. F.; Albracht, S. P. J. *Biochemistry* **2004**, *43*, 6820−6831.
(31) Stadler, C.; De Lacey, A. L.; Montet, Y.; Volbeda, A.; Fontecilla-Camps, J. C.; Conesa, J. C.; Fernandez, V. M. *Inorg. Chem.* **2002**, *41*, 4424−4434.
(32) George, S. J.; Kurkin, S.; Thorneley, R. F.; Albracht, S. P. J. *Biochemistry* **2004**, *43*, 6808−6819.
(33) De Lacey, A. L.; Pardo, A.; Fernandez, V. M.; Dementin, S.; Adryanczyk-Perrier, G.; Hatichikian, E. C.; Rousset, M. *J. Biol. Inorg. Chem.* **2004**, *9*, 636−642.
(34) van der Zwaan, J. W.; Albracht, S. P. J.; Fontijn, R. D.; Roelofs, Y. B. M. *Biochim. Biophys. Acta* **1986**, *872*, 208−215.
(35) Cammack, R.; Patil, D. S.; Hatchikian, E. C.; Fernandez, V. M. *Biochim. Biophys. Acta* **1987**, *912*, 98−109.
(36) van der Zwaan, J. W.; Coremans, J. M.; Bouwens, E. C.; Albracht, S. P. J. *Biochim. Biophys. Acta* **1990**, *1041*, 101−110.
(37) Bagley, K. A.; Vangarderen, C. J.; Chen, M.; Duin, E. C.; Albracht, S. P. J.; Woodruff, W. H. *Biochemistry* **1994**, *33*, 9229−9236.
(38) Davidson, G.; Choudhury, S. B.; Gu, Z.; Bose, K.; Roseboom, W.; Albracht, S. P. J.; Maroney, M. J. *Biochemistry* **2000**, *39*, 7468−7479.
(39) De Lacey, A. L.; Stadler, C.; Fernandez, V. M.; Hatchikian, E. C.; Fan, H.-J.; Li, S.; Hall, M. B. *J. Biol. Inorg. Chem.* **2002**, *7*, 318−326.
(40) Ogata, H.; Mizoguchi, Y.; Mizuno, N.; Miki, K.; Adachi, S.; Yasuoka, N.; Yagi, T.; Yamauchi, O.; Hirota, S.; Higuchi, Y. *J. Am. Chem. Soc.* **2002**, *124*, 11628−11635.
(41) Adams, M. W. W. *Biochim. Biophys. Acta* **1990**, *1020*, 115−145.
(42) Hallahan, D. L.; Fernandez, V. M.; Hatchikian, E. C.; Hall, D. O. *Biochimie* **1986**, *68*, 49−54.
(43) Zorin, N. A. *Biochimie* **1986**, *68*, 97−101.
(44) De Lacey, A. L.; Santamaria, E.; Hatchikian, E. C.; Fernandez, V. M. *Biochim. Biophys. Acta* **2000**, *1481*, 371−380.
(45) Heering, H. A.; Weiner, J. H.; Armstrong, F. A. *J. Am. Chem. Soc.* **1997**, *119*, 11628−11638.

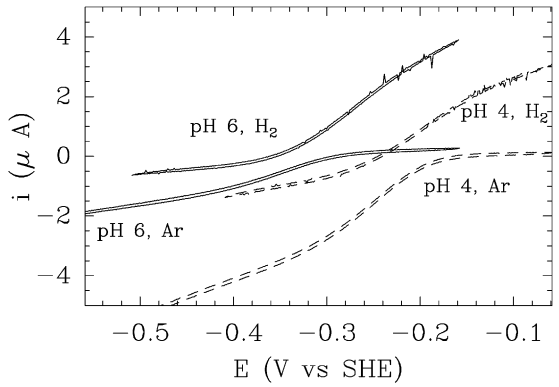

Figure 1. Steady-state cyclic voltammograms for Df-hase adsorbed at a PGE electrode. These were recorded with a single film of enzyme successively transferred into solutions at pH 6 (plain lines) or 4.1 (dashed lines), flushed with either H_2 or Ar, as indicated. $T = 40$ °C; scan rate, $\nu = 20$ mV/s; electrode rotation rate, $\omega = 2$ krpm.

All PFV experiments were carried out in a glovebox (Jacomex) under an N_2 atmosphere ($O_2 < 1$ ppm). The electrochemical cell, thermostated at 40 °C using a water circulation, was housed in a Faraday cage. A pyrolytic graphite edge (PGE) rotating disk working electrode (area $A \approx 3$ mm^2) was used in conjunction with an EG&G M636 electrode rotator, a platinum wire was used as a counter electrode, and a saturated calomel electrode (SCE), located in a Luggin sidearm containing 0.1 M NaCl and maintained at room temperature, was used as a reference. All potentials are quoted versus the standard hydrogen electrode (SHE), $E_{SHE} = E_{SCE} + 241$ mV at room temperature. Cyclic voltammetry (whereby the electrode potential is sweeped and the current is measured), chronoamperometry (the electrode potential is stepped, and the current is measured), and chronopotentiometry (the current is constant, and the electrode potential is measured) experiments were performed with an Autolab electrochemical analyzer (PGSTAT 12, Eco Chemie) equipped with a staircase scan generator. Cyclic voltammograms were recorded in digital mode, with a fractional sampling time of 1, to minimize the capacitive current.

Before preparation of an enzyme film, the PGE electrode was polished with an aqueous alumina slurry (Buehler, 1 μm) and sonicated thoroughly. Protein films were prepared by painting the electrode with about 0.5 μL of a stock solution of enzyme (≈20 μM in 50 mM HEPES·Na, pH 8). The electrode was inserted into the cell containing about 3 mL of buffer at 40 °C and cycled repeatedly until the enzyme was activated and a stable current response was obtained. The enzyme-coated electrode could then be transferred into solutions of different pH with very little loss in electroactive coverage.

The electrochemical cell was always continuously flushed with H_2, Ar, or a mixture of 10% H_2 and 90% N_2 (all from Air Liquide), using a cannular to bubble the gas directly into the cell solution. The same buffer as that present in the electrochemical cell, but saturated with H_2, CO, or air at 40 °C (with the safety precautions relevant to the high toxicity of carbon monoxide), was kept in a capped serum bottle and thermostated at 40 °C using a bain-marie in the glovebox. Small aliquots of this solution were injected into the electrochemical cell using gastight syringes. We shall note x the volumic fractions that refer to the amount of solution injected: x is the volume injected divided by total volume of solution in the cell after the injection; it is also the ratio of the concentration of gas at time of injection over the concentration under saturating conditions, $x = C(t = 0)/C(\text{sat})$.

Results

Steady-State Activity: Comparison with the Enzyme from *A. vinosum*. Figure 1 shows steady-state, catalytic voltammograms for Df-hase adsorbed at a PGE electrode, recorded at $T = 40$ °C, pH 4 (dashed lines) and 6 (plain lines), under an atmosphere of either Ar or H_2, as indicated. The films were very stable and could be used for several hours. No noncatalytic signals were observed, suggesting[11] that the electroactive coverage is low, below 3 pmol/cm^2. Thus, the absolute turnover number cannot be determined from our data.

The shapes of the voltammograms for H_2 oxidation and evolution by adsorbed Av-hase have been thoroughly discussed in refs 11−16; only a brief description of the signals shown in Figure 1 is included below, with emphasis on the differences between Av- and Df-hases.

The voltammograms for Df-hase recorded under an atmosphere of argon are discussed first (Figure 1). A reductive (negative) current is measured which results from catalytic proton reduction at the active site and continuous electron transfer from the electrode to the enzyme. The activity increases (the current becomes more negative) when the electrode potential is low enough that the catalytic state competent for evolving H_2 is formed. Thus we may expect the catalytic wave to be sigmoidal, with a midwave potential that equates the reduction potential of the Ni−C/Ni−R couple.[46] However, the current does not level off at high driving force (low electrode potential); this was also observed with Av-hase and interpreted in terms of a dispersion of enzyme orientations on the electrode, resulting in a dispersion of interfacial electron-transfer rates.[13,14] Despite this complication, the position of the reductive wave does relate to the reduction potential of the Ni−C/Ni−R redox transition,[46] and from the position of the voltammograms recorded under Ar at pH 4 and 6 (Figure 1), it is obvious that this reduction potential decreases by about 60 mV per pH unit, showing that the reduction of Ni−C is coupled to the uptake of one proton. The change in overall magnitude of the current is simply related to the change in activity with pH: under 1 atm of Ar, the enzyme turns over about 3 times faster at pH 4 than at pH 6, as observed with Av-hase.[13] Similarly to Av-hase again, the reductive current measured under Ar is slightly dependent on electrode rotation rate ω (data not shown): this results from product H_2 accumulating near the electrode surface at low rotation rate, thus inhibiting H_2 evolution.[13]

When the voltammograms are recorded under an atmosphere of H_2, the catalytic current is positive at high potential and negative at low potential and results from H_2 oxidation or evolution, under conditions where the active site is oxidized or reduced, respectively. The reductive current is lower than that recorded under Ar because of H_2 inhibition of proton reduction, as mentioned above, but in contrast with the results for Av-hase,[13] inhibition of proton reduction by Df-hase is not complete under 1 atm of H_2. Remarkably, the oxidative activity is about the same at pH 4 and 6 (Figure 1) and is nearly unchanged at pH values as high as 9 (data not shown). This is in agreement with the PFV study of the enzyme from *A. vinosum*[13] and contrasts with the bell-shaped change in oxidative

(46) To relate the position of the reductive wave to a reduction potential of the active site, two limiting cases can be considered, depending on whether $E^0_{SI/C}$ is lower or greater than $E^0_{C/R}$ (see the detailed discussion in the appendix of ref 13). The analysis of the wave shape (not shown) shows that $E^0_{C/R} < E^0_{SI/C}$; therefore, when Ni−R is formed at $E \lesssim E^0_{C/R}$, the electrode potential is already low enough with respect to $E^0_{SI/C}$ that the rate of reduction of SI no longer affects turnover. Thus the exact value of $E^0_{SI/C}$ has little influence on the wave shape, which is relatively broad ("one-electron") and centered on $E^0_{C/R}$.

activity that is measured in solution assays.[9] This difference has been interpreted in terms of the oxidation of the enzyme by soluble dyes limiting the rate of turnover in solution assays.[3,11−13,16]

Under an atmosphere of H_2, a moderately high electrode rotation rate ($\omega = 2$ krpm) was always enough to ensure that mass transport did not limit the current (increasing the electrode rotation rate further did not increase the oxidation current); this is unlike the case of Av-hase.[17] Mass transport control arises when the electrode coverage and the activity are so high that substrate consumption by the enzyme results in its depletion near the electrode surface.[11] The fact that mass transport control is not observed in the case of Df-hase results most likely from this enzyme being less active and/or adsorbed with a lower electroactive coverage than Av-hase; this is consistent with the observation that the measured currents are lower than those obtained with Av-hase.[47] As a rule, mass transport control hides the interesting features of the voltammograms, and the fact that these limitations are released at moderate electrode rotation rate in the case of Df-hase is certainly an advantage.

Figure 1 shows that, under 1 atm of H_2, Df-hase catalyzes both H_2 uptake and evolution. At $E \approx -230$ mV (at pH 4) and -350 mV (pH 6), the oxidative and reductive contributions to the current exactly balance each other and there is no net current. The value of this "open circuit potential" (OCP) is such that the H^+/H_2 transformation is at equilibrium and the enzyme does not catalyze any net transformation: the OCP equates the formal reduction potential of the substrate/product couple[12,18,48−50] and does not characterize the enzyme.

Figure 1 shows that Df-hase is an efficient catalyst of both H_2 evolution and uptake. This contrasts with the enzyme from *A. vinosum*, which is strongly biased in the oxidative direction (with Av-hase, the catalytic current for H^+ reduction is at best 10 times smaller than that for oxidative activity).[12,13]

Principle of the Transient Measurements. Hereafter, we analyze the change in enzyme activity as a function of time, following the injection of a small amount of solution saturated with H_2, CO, or air (substrate or inhibitor) into the solution in contact with the enzyme. The cell solution being continuously flushed with either H_2 or Ar (by bubbling the gas directly into the cell), the added, dissolved gas "escapes" from the solution, and its concentration drops back to zero within a few minutes following the injection. Importantly, this decay is exponential, as demonstrated below by the results of two independent experiments (Figure 2).

When a polished graphite electrode is poised at low potential (negative with respect to SHE at neutral pH) and rotated (to maintain steady-state mass transport) in a solution, a reductive (negative) current i can be measured, which is proportional to the concentration of dissolved oxygen. Figure 2A shows this reduction current as a function of time following the injection at time $t \approx 50$ and 300 s of an air-saturated solution in an electrochemical cell flushed with Ar. The dead time for mixing

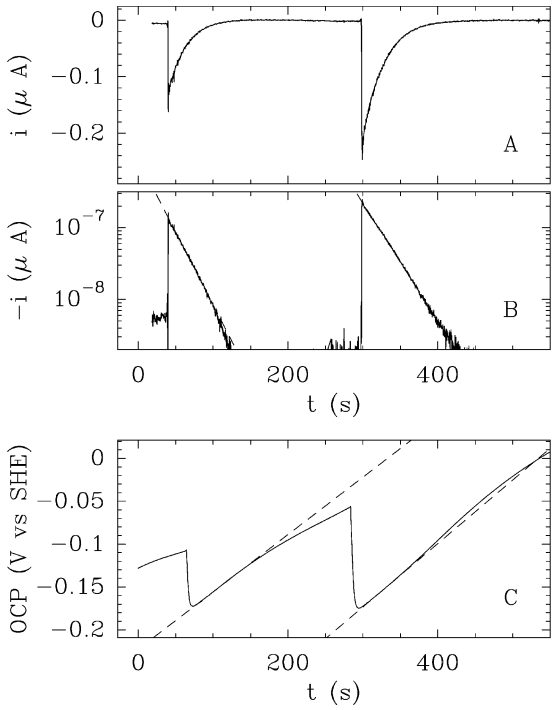

Figure 2. (Panels A and B) Decay of the current resulting from oxygen reduction after injection in a cell flushed with Ar or a small amount of air-saturated solution, with volumic fractions $x = 3.2 \times 10^{-2}$ and $x = 6.05 \times 10^{-2}$. $\omega = 2$ krpm. $E = -260$ mV. The slopes $-1/(2.3\tau)$ of the semilog plots gave $\tau \approx 20$ s. (Panel C) Relaxation of the open circuit potential of a hydrogenase-coated electrode following the injection of an H_2-saturated solution in the cell flushed with Ar. $x = 3.3 \times 10^{-3}$ and $x = 6.6 \times 10^{-3}$. The slopes $RT/2F\tau$ of the linear parts of the data (dashed lines) gave $\tau \approx 20$ s. pH 4.15, $\omega = 2$ krpm, $T = 40$ °C.

is smaller than 0.5 s. The linear plot of $\log(-i)$ against t in panel B demonstrates that the time-dependent oxygen bulk concentration follows

$$C(t) = C(0)\exp(-t/\tau) \qquad (1)$$

No significant deviation from an exponential decay is observed while the current (and thus the bulk concentration of oxygen) decreases over 2 orders of magnitude. The relaxation time, τ, depends mainly on the flow of neutral gas which is bubbled through the cell solution; it was also found to increase with the volume of solution in the cell and to decrease with increasing electrode rotation rate (increasing ω from 500 to 7 krpm resulted in a 10-fold decrease in τ).

The result of a distinct, zero-current experiment also shows that the concentration of added gas decreases exponentially with time: inject some H_2-saturated solution in an electrochemical cell continuously flushed with Ar and measure the time-dependent open circuit potential (OCP) of an electrode onto which hydrogenase is adsorbed. The OCP equates the formal H^+/H_2 reduction potential, which depends on H_2 concentration according to the Nernst equation. Thus, as a result of the exponential decrease in H_2 concentration, the OCP increases linearly with time, with slope $\mathrm{dOCP/d}t = RT/2F\tau$, as indeed observed in Figure 2C. In the next section, we show that such slow and well-defined change in H_2 concentration against time can be used to determine how activity depends on substrate concentration.

(47) This could also result from Df-hase having a smaller Michaelis constant than Av-hase, so that Df-hase would remain saturated despite H_2 depletion.

(48) Hirst, J.; Sucheta, A.; Ackrell, B. A. C.; Armstrong, F. A. *J. Am. Chem. Soc.* **1996**, *118*, 5031−5038.
(49) Léger, C.; Heffron, K.; Pershad, H. R.; Maklashina, E.; Luna-Chavez, C.; Cecchini, G.; Ackrell, B. A. C.; Armstrong, F. A. *Biochemistry* **2001**, *40*, 11234−11245.
(50) Zu, Y.; Shannon, R. J.; Hirst, J. *J. Am. Chem. Soc.* **2003**, *125*, 6020−6021.

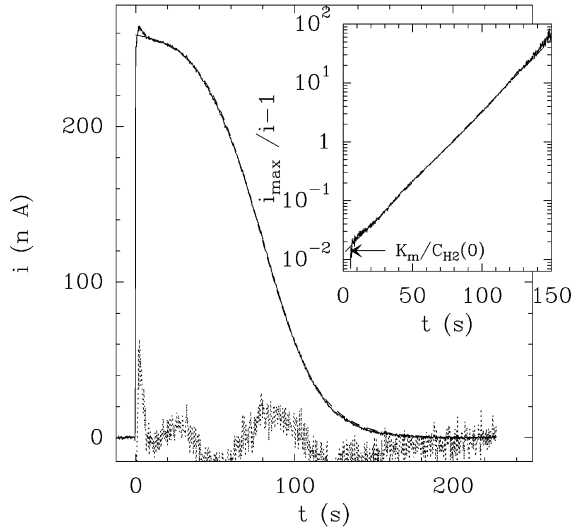

Figure 3. Catalytic, sigmoidal, transient current for hydrogen oxidation by Df-hase, following the injection of a solution saturated with hydrogen in the electrochemical cell flushed with Ar. pH 6.1, $E = -160$ mV, $T = 40$ °C, $x = 0.8$, $\omega = 2$ krpm, $\tau \approx 18$ s. Dotted line: residual, enlarged 10 times, after the data were fit to eq 2 (dashed line). Inset: the log transform of the transient, fitted to a straight line according to eq 3.

Measurements of Michaelis Constants for H_2 Oxidation. Figure 3 shows a current versus time plot for H_2 oxidation by adsorbed hydrogenase, following the injection into the cell flushed with Ar of an H_2-saturated buffer, while the electrode potential is poised at a value which favors the presence of the Ni−SI state. Provided that (i) the activity (and thus the catalytic current) depends on H_2 concentration according to the Michaelis−Menten equation and that (ii) the H_2 concentration decreases exponentially with time according to $C_{H_2}(t) = C_{H_2}(0)\exp(-t/\tau)$, the current transient that follows the injection of H_2 is expected to be sigmoidal

$$i(t) = \frac{i_{max}}{1 + \frac{K_m}{C_{H_2}(0)}\exp(t/\tau)} \qquad (2)$$

as indeed observed in Figure 3, where the best fit to eq 2 and the residue enlarged 10 times are plotted with dashed and dotted lines, respectively. The current is nearly constant during the few seconds that follow the injection of H_2-saturated buffer, when the H_2 concentration is still large enough to saturate the enzyme; thus, in this experiment, the initial current is a "maximal" current (just as v_{max} relates to turnover under saturating conditions in Michaelis−Menten kinetics).

The sigmoidal shape of the transient is easily demonstrated in the semilog plot of $i_{max}/i - 1$ against t (inset of Figure 3),

$$\log_{10}\left(\frac{i_{max}}{i(t)} - 1\right) = \log_{10}\frac{K_m}{C_{H_2}(0)} + \frac{t}{2.3\tau} \qquad (3)$$

and the value of K_m can be determined directly from the y-intercept of the log transform: $K_m = (6.5 \pm 3) \times 10^{-3}$ atm of H_2 (≈5 μM); this is estimated from the results of multiple runs. In the case of NiFe-hases, published values of K_m range from 0.07 to 11 μM (refs 51−54).

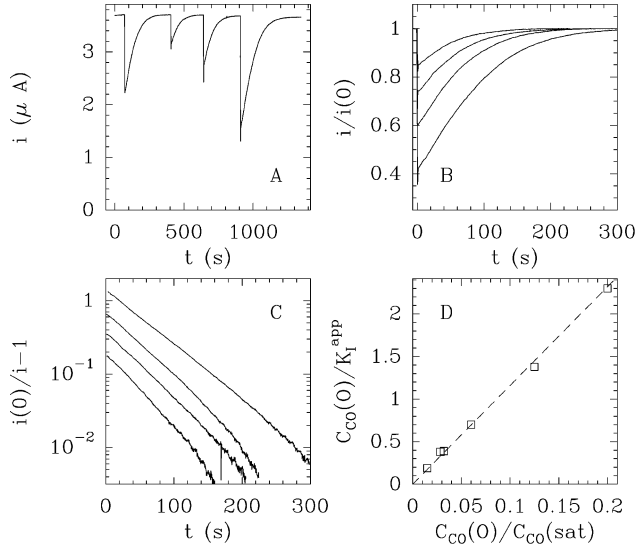

Figure 4. CO inhibition of H_2 oxidation by adsorbed NiFe hydrogenase. (A) Current transients following the injection of CO-saturated solutions ($x = 6 \times 10^{-2}$, 1.5×10^{-2}, 2.25×10^{-2}, and 1.25×10^{-1}) to a solution flushed with H_2. pH 6.3, $E = -160$ mV. $\omega = 2$ krpm, $\tau \approx 50$ s. (B) current i normalized by its value just before CO was added, $i(0)$. (C) log transforms of the transients, eq 7. (D) The plot of the y-intercepts of the log transforms against x is fitted to a straight line (dashed).

CO Inhibition of H_2 Oxidation under 1 atm of H_2. Figure 4 illustrates the method that was used to measure the dissociation constant corresponding to CO inhibition of H_2 oxidation. The enzyme-coated electrode was poised at $E = -160$ mV, in a solution at pH 6, flushed with H_2. A steady, positive current is measured which is proportional to the rate of H_2 oxidation. At repeated times, we injected small volumes of CO-saturated solution (the volumic fractions x are given in the figure caption). The current dropped instantaneously each time CO was added (panel A), and activity was recovered over the next ≈300 s while the concentration of dissolved CO decayed exponentially. The fact that the activity is fully recovered after CO has vanished from the cell demonstrates that the electrode potential was too low to result in the oxidation of the active site to its inactive form Ni−B.

In the following, we use the notation K_I(inhibitor/substrate) for the inhibition constants. For example, $K_I(CO/H_2)$ is the dissociation constant for the inhibition of H_2 oxidation by CO. Since CO is a competitive inhibitor of H_2,[42,43] the activity depends on CO and H_2 concentrations according to the relationship[55]

$$i(t) = \frac{i_{max}}{1 + \frac{K_m}{C_{H_2}(t)}\left(1 + \frac{C_{CO}(t)}{K_I(CO/H_2)}\right)} \qquad (4)$$

Its dependence on C_{CO} (and time) is simple if the H_2 concentration remains constant during the transient (this is expected to

(51) Colbeau, A.; Vignais, P. M. *Biochim. Biophys. Acta* **1981**, *662*, 271−284.
(52) Vignais, P. M.; Henry, M. F.; Berlier, Y.; Lespinat, P. A. *Biochim. Biophys. Acta* **1982**, *681*, 519−529.
(53) Meuer, J.; Bartoschek, S.; Koch, J.; Kü×b9nkel, A.; Hedderich, R. *Eur. J. Biochem.* **1999**, *265*, 325−335.
(54) Keefe, R. G.; Axley, M. J.; Harabin, A. L. *Arch. Biochem. Biophys.* **1995**, *317*, 449−456.
(55) Cornish-Bowden, A. *Fundamental of Enzyme kinetics*; Portland Press: 2004.

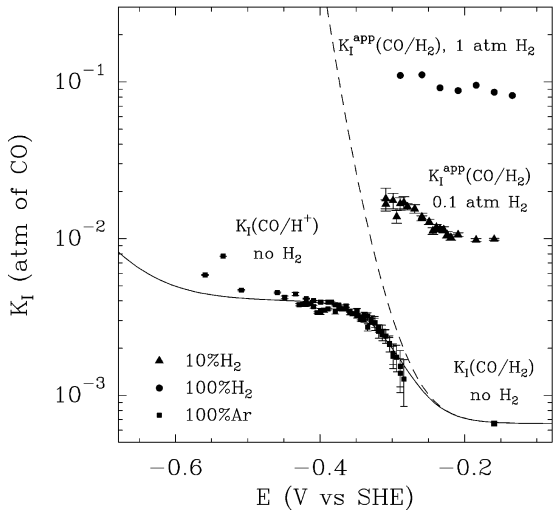

Figure 5. Summary of all the constants for the inhibition by CO of H_2 uptake and evolution by Df NiFe hase, at pH 6, 40 °C. Values of $K_I^{app}(CO/H_2)$ measured under 1 atm of H_2 (●, upper right corner) and 0.1 atm of H_2 (▲), and the corresponding value of $K_I(CO/H_2)$ once the competition with H_2 was accounted for (lower right corner). (■ on the left) $K_I(CO/H^+)$, and the lines are from eq S5; see text.

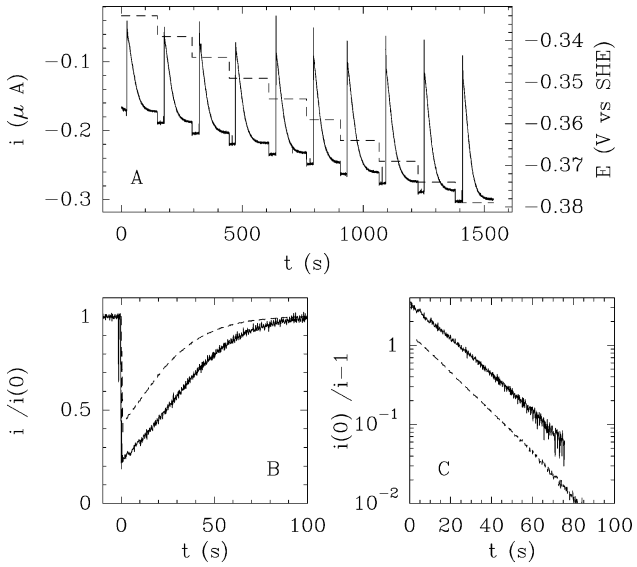

Figure 6. Measurement of the dependence of $K_I(CO/H^+)$ on the driving force. (Panel A) Potential stair case applied to the electrode (dashed line and right *y*-axis) and proton reduction current following the injection of minuscule amounts of CO saturated solutions (plain line and left axis). (Panel B) Normalized current transients recorded at $E = -460$ (dashed line) and -290 mV (plain line). (Panel C) Same transients after the log transform was applied. pH 6, 40 °C, 1 atm of Ar, $\omega = 2$ krpm, $\tau \approx 18$ s.

be the case if the fraction of added CO-saturated solution is small)

$$i(t) \approx \frac{i(0)}{1 + \dfrac{C_{CO}(0)\exp(-t/\tau)}{K_I^{app}(CO/H_2)}} \qquad (5)$$

where $i(0) = i_{max}/(1 + K_m/C_{H_2})$ is the current just before the addition of CO, and

$$K_I^{app}(CO/H_2) = K_I(CO/H_2)\frac{C_{H_2}}{K_m}\left(1 + \frac{K_m}{C_{H_2}}\right) \qquad (6)$$

Under saturating conditions ($C_{H_2} \gg K_m$), the apparent inhibition constant is proportional to the concentration of H_2.

The sigmoidal transient predicted by eq 5 is made linear in Figure 4C, using the following log transform:

$$\log_{10}\left(\frac{i(0)}{i(t)} - 1\right) = \log_{10}\frac{C_{CO}(0)}{K_I^{app}} - \frac{t}{2.3\tau} \qquad (7)$$

The *y*-intercepts of the plots in Figure 4C gave the values of $C_{CO}(0)/K_I^{app}$ which were found to be proportional to *x*, as expected (panel D). [*x* is the volumic fraction of saturated solution injected at $t = 0$ and thus equates $C(0)/C(sat)$.] The value of $K_I^{app}(CO/H_2) \approx 0.1$ atm was determined from the slope of the straight line in Figure 4D. Taking into account the competition with H_2 (eq 6) gave $K_I(CO/H_2) \approx 6.6 \times 10^{-4}$ atm of CO ($\approx$0.65 μM).

The experiments were repeated for several values of the electrode potential *E* (data not shown). The corresponding values of $K_I^{app}(CO/H_2)$ are collected in Figure 5 (circles, upper right corner): under 1 atm of H_2, we did not detect any significant dependence on *E*.

CO Inhibition of H_2 Oxidation under 0.1 atm of H_2. Similar experiments were carried out flushing the cell with a mixture of 10% H_2 and 90% N_2 (data not shown). Consistently with the fact that CO and H_2 compete for binding to the active site, the value of $K_I^{app}(CO/H_2)$ decreased about 10 times when the H_2 pressure was decreased from 1 to 0.1 atm (filled triangles in Figure 5). A slight increase in $K_I^{app}(CO/H_2)$ was observed as the electrode potential was decreased.

H_2 Inhibition of Proton Reduction under 1 atm of Ar. Similar experiments allowed the inhibition of proton reduction by hydrogen to be studied: the cell is flushed with Ar, the electrode is poised at low potential, a negative current resulting from proton reduction by the enzyme is measured, which decreases (becomes less negative) when a H_2-saturated solution is injected in the cell. Typical results are shown in the Supplementary Information (Figure S1). We found $K_I(H_2/H^+) \approx 0.2$ atm of H_2 at pH 6, $E = -660$ mV, and 0.23 atm at pH 4, $E = -560$ mV.

CO Inhibition of Proton Reduction under 1 atm of Ar and Its Dependence on Electrode Potential. Figure S2 (Supporting Information) shows typical results corresponding to the addition of CO-saturated solutions to a cell flushed with Ar while the enzyme catalyzes the evolution of H_2 at low electrode potential. The value of $K_I(CO/H^+)$ measured from these experiments (Figure S2D) was found to depend on the electrode potential, and a systematic study was undertaken. The fact that there is little noise in the linear plots of $C(0)/K_I$ against *x* in Figures 4D, S1D, and S2D suggests that the value of the inhibition constant can be determined with good accuracy from the analysis of a single transient; this made very convenient the study of the dependence of $K_I(CO/H^+)$ on *E*, as illustrated in Figure 6: the electrode potential was stepped with time as exemplified by the dashed line in panel A; after each step, very small volumes of CO-saturated solution ($x \leq 10^{-2}$) were added, and the current was monitored simultaneously (plain line in panel A). Potential ramps were performed in either direction, the cell solution was renewed several times, and the steady increase in cell volume resulting from the addition of small

volumes of CO-saturated solution was accounted for to avoid systematic errors. Normalized transients, recorded at $E = -460$ (dashed line) and -290 mV (plain line) are plotted in panels B and C, from which it is obvious that the inhibitory effect of CO is more pronounced at higher electrode potential. The values of $K_I(CO/H^+)$ measured from each transient are collected in Figure 5 (filled squares). The errors at high electrode potential result from the catalytic current becoming so small that the value of the inhibition constant is increasingly dependent on the presence of a small current offset (the limits of the intervals given for each measurement were obtained by analyzing the data either with no correction or after they have been shifted by +20 nA).

Modeling the Dependence of $K_I(CO/H^+)$ on *E*. To interpret the dependence of the inhibition constant on driving force under reducing conditions, we consider that the oxidized, active form of the active site, Ni−SI, is reduced in two successive one-electron steps (via the intermediate oxidation level Ni−C) to Ni−R, which is protonated and releases H_2 with a rate k_2 (Scheme S3 in the Supporting Information). Electron-transfer rates are described by the Butler−Volmer equation.[13] Binding of CO to Ni−SI results in the formation of the dead-end species termed Ni−SI−CO; the reasons why we assume that CO only binds to Ni−SI are given in the Discussion. The equation for the catalytic, reductive current (eq S3), is easily derived as a function of the electrode potential and four parameters: the ratio C_{CO}/K_{SI} (where K_{SI} is the dissociation constant from Ni−SI), the reduction potentials of the SI/C and C/R couples, and the ratio k_2/k_0, which describes the competition between turnover and interfacial electron transfer. The ratio of the current in the presence of CO to that in the absence of CO simplifies to

$$\frac{i}{i(0)} = \frac{1}{1 + \dfrac{C_{CO}}{K_I(CO/H^+)}} \qquad (8)$$

with an inhibition constant $K_I(CO/H^+)$ (eq S5) which depends on E and four parameters: K_{SI}, two reduction potentials, and k_2/k_0.

The best fit of $K_I(CO/H^+)$ in Figure 5 to eq S5 (plain line), with K_{SI} fixed to the value of $K_I(CO/H_2)$ determined above, gave $E^0_{SI/C} = -270$ mV, $E^0_{C/R} = -360$ mV, and $k_2/k_0 = 10^{2.5}$. The values of these reduction potentials are very close to those determined from the analyses of the catalytic waves recorded at the same pH (Figure 1): $E^0_{SI/C} = -290$ mV, and $E^0_{C/R} = -340$ mV at pH 6. The dashed line in Figure 5 was obtained with the same parameters except for the value of k_2/k_0 that was set to zero to illustrate the fully reversible limit,[49] where the concentations of the redox species are simply related to $E^0_{SI/C}$, $E^0_{C/R}$, and E by the Nernst equation.

Aerobic Inactivation. To measure the decrease in rate of H_2 oxidation that results from the injection in the cell of an O_2-containing solution, care must be taken that direct reduction of O_2 on the electrode does not interfere with the activity measurement; this would result in a contribution to the measured current (Figure 2A) that could not be simply subtracted. Thus, all aerobic inactivation experiments reported below were performed by poising the electrode potential at a value which was high enough that no direct O_2 reduction occurred ($E > 0$ mV at pH 7). At such high potential, the enzyme inactivates slowly as a result of its transformation to Ni−B.[15] In contrast with the experiments reported above, the decrease in activity that results from the injection of O_2 is therefore superimposed on a slow decay resulting from the anaerobic inactivation.

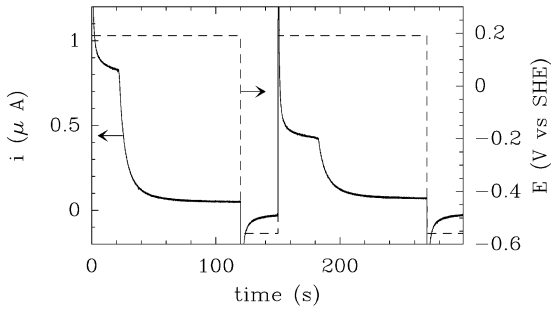

Figure 7. O_2 inhibition of H_2 oxidation. Dashed line and right *y*-axis: potentiel steps applied to measure the rate of H_2 oxidation in the presence of O_2 and subsequently reactivate the enzyme. Plain line and left axis: current transients; aliquots of air saturated solutions ($x = 3.2 \times 10^{-2}$ and 1.6×10^{-2}) were added at $t = 20$ and 180 s. 1 atm of H_2, pH 7, 40 °C, $\omega = 2$ krpm.

Figure 7 illustrates the procedure that was used to measure the rate of aerobic inactivation. The electrode was poised at 190 mV, a catalytic current for H_2 oxidation by adsorbed hydrogenase was measured, and an aliquot of air-saturated solutions was injected (at time $t = 20$ s). In contrast with inhibition by CO, the decrease in current following the addition of O_2 can be resolved, and activity is not recovered under oxidizing conditions, even after oxygen vanishes from the cell solution. The electrode potential was then poised at -560 mV for 30 s to reactivate the enzyme.[56] When the electrode potential was stepped back at 190 mV (at $t = 150$ s in Figure 7), about half of the activity was recovered, so that subsequent measurements of inactivation kinetics could be carried out with the same film.

To measure the rate of aerobic inactivation from such data, we consider that the concentration of active enzyme decays as a result of two competitive processes: (i) an O_2-independent oxidation to Ni−B, with first-order rate constant k_b and (ii) an O_2-dependent, bimolecular process with an apparent first-order rate constant $k_a \times C_{O_2}(t)$ which decreases exponentially with time as O_2 vanishes from the cell. The differential equation that describes the change in concentration of active enzyme Γ reads

$$\frac{d\Gamma}{dt} = -[k_b + k_a C_{O_2}(0) \exp(-t/\tau)]\Gamma \qquad (9)$$

Since the catalytic current i is proportional to Γ, eq 9 is rewritten in a form that is convenient to analyze the data in Figure 8A:

$$\frac{d \ln i}{dt} = -k_b - k_a \times C_{O_2}(0) \exp(-t/\tau) \qquad (10)$$

where $d \ln i/dt$ has very simple physical meaning: it is the apparent first-order rate of inactivation, which depends on the instant concentration of bulk O_2.

Figure 8B shows the first derivatives of the natural logarithm of the current transients plotted in panel A, fitted to the exponential variation predicted by eq 10 (dots). Three parameters were adjusted to fit each transient: k_b, $k_a C_{O_2}(0)$, and τ. It is

(56) Care was taken that no O_2 was left in the cell before stepping the electrode at low potential, as the products of direct O_2 reduction on the electrode may damage irreversibly the enzyme.

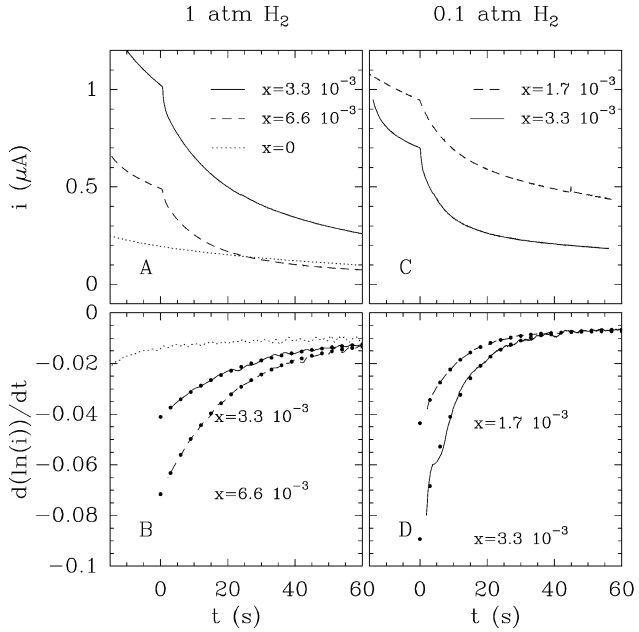

Figure 8. (Panels A and C) Decrease in the rate of H_2 oxidation by Df-hase resulting from the injection at time $t = 0$ of small amounts of aerated buffer into the cell, while the electrode is poised at high potential. (Panel A) 1 atm of H_2, $\tau \approx 24$ s. (Panel C) 0.1 atm of H_2, $\tau \approx 10$ s, $E = 190$ mV, pH 6.8, 40 °C, $\omega = 2$ krpm. (Panels B and D) Plots of d(ln(*i*))/d*t* against time, and fits to eq 10 (●).

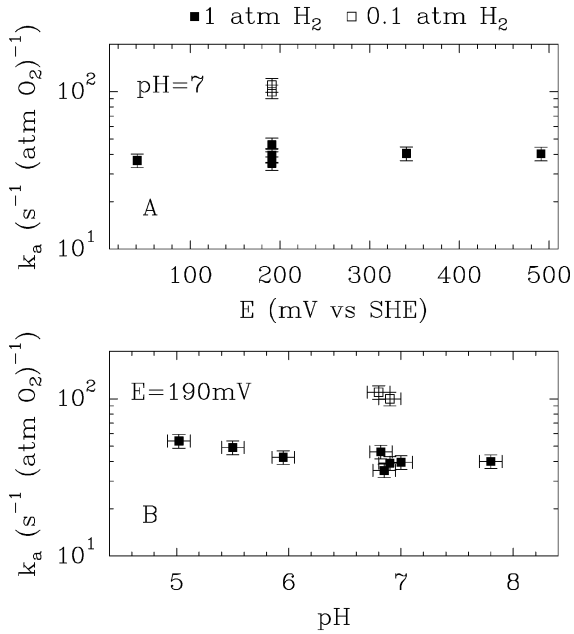

Figure 9. Dependence of the inactivation rate constant on *E* at pH 6.9 ± 0.1 (Panel A) and on pH at $E = 190$ mV (Panel B). $T = 40$ °C, 1 atm of H_2 (■) or 0.1 atm of H_2 (□), $\omega = 2$ krpm.

obvious from the data that the values of τ and k_b are about the same for both transients, while the value of $k_a C_{O_2}(0)$ (the magnitude of the decay of d ln *i*/d*t*) is proportional to the initial concentration of O_2, as expected. This and the fact that the change in d ln *i*/d*t* against time is exponential[57] confirm that the aerobic inactivation is a bimolecular process.

The fraction of O_2 in the air being ≈20%, we obtained $k_a = 38 \pm 4$ s^{-1} (atm O_2)$^{-1}$ ($k_a \approx 3 \times 10^4$ s^{-1} M^{-1}) at $E = 190$ mV, pH 7, 40 °C, 1 atm of H_2 (this was estimated from seven independent data sets such as those in Figure 8). The value of the first-order rate constant k_b corresponding to the anaerobic inactivation was estimated to be ≈10^{-2} s^{-1}. Consistent with the FTIR study of Df-hase in ref 33, and in contrast with the results obtained with the enzyme from *A. vinosum*,[15] we did not observe any significant pH-dependence for the rate of anaerobic inactivation. This difference between the two enzymes remains to be explained.

Dependence of the Rate of Aerobic Inactivation on H_2 Pressure, *E*, and pH. All things being equal, the bimolecular rate constant for aerobic inactivation was increased to 105 ± 15 s^{-1} (atm O_2)$^{-1}$ when the experiment was performed under 0.1 atm of H_2 instead of 1 atm of H_2 (panels C and D in Figure 8).

To determine whether the electrode potential and the pH value have an influence on the rate of the inactivation process, experiments such as those in Figure 8 were repeated, under 1 atm of H_2, either at pH 7 changing the value of *E* or at $E = 190$ mV as a function of pH. The results are collected in Figure 9.

Discussion

For the past five years, PFV studies of Av-hase have given interesting insights into the catalytic properties of NiFe enzymes.[11−16] The fact that this technique allows the measurement of activity over a large range of driving force and can be used to determine how activity evolves with time following an instant change in redox conditions makes it specially suitable to study the complex redox and redox-coupled processes that occur in NiFe hydrogenases over very different time scales. Here, the first PFV study of Df-hase generalizes some important conclusions that were drawn from the experiments with the *A. vinosum* enzyme (regarding how activity depends on pH[13]) and gives further information about the binding and aerobic inactivation kinetics in NiFe hydrogenases.

Transient Measurements: H_2 Binding and CO Inhibition. In this work, we have measured by PFV the activity of hydrogenase as a function of the concentration of dissolved substrate or inhibitor. Instead of using a closed electrochemical cell (with the atmosphere above the solution sealed from that of the glovebox, set to the desired composition, and allowed to equilibrate with the buffer), we propose an original technique that consists of equilibrating the buffer with H_2 or Ar (by continuously bubbling gas into the cell) and then adding quickly (within a fraction of a second) an aliquot of buffer saturated with CO, H_2, or air. Following the injection, within a few minutes, the cell solution reequilibrates with the atmosphere of the glovebox, and the enzyme turnover can be measured as a function of time, while the substrate or inhibitor vanishes from the cell solution.

Importantly, the fact that the decrease in inhibitor or substrate concentration over time is exponential (as demonstrated by the experiments in Figure 2) makes it very easy to obtain the relation between concentration and steady-state activity in a single, time-

(57) If the inactivation had to be interpreted in terms of binding of O_2 with dissociation constant K_I before the inactivation proceeds with a rate constant k_a^{max}, this should appear from the data as a sigmoidal (as opposed to exponential) change against time

$$\frac{d\ln i}{dt} = -k_b - \frac{k_a^{max}}{1 + \frac{K_I}{C_{O_2}(0)}\exp(t/\tau)} \qquad (11)$$

The fact that the initial rate of aerobic inactivation is proportional to *x* is merely an additional check that, under the experimental conditions we used, it is first-order in O_2.

dependent measurement: in the case of the reversible binding of substrate H_2 or inhibitor CO, the hyperbolic dependence of activity on a concentration that decreases exponentially with time results in sigmoidal transients that can be easily analyzed using log transforms.

In the case of the transient experiments described in this paper, changing the electrode rotation rate ω had an influence on the relaxation time τ, but this did not influence the measured dissociation and Michaelis constants (data not shown). This implies that the changes in concentrations were always slow enough (with respect to turnover rate) that steady-state conditions applied at all times; therefore steady-state rate equations could be used to model the transients.

This experimental approach contrasts with both traditional assays[55] (where initial rates are measured for discrete values of the substrate concentration) and integral methods, where the turnover rate changes as a function of time following the consumption of the substrate by the enzyme, in which case kinetic equations must be integrated to account for the time courses of reactions.[58,59] Indeed, in the experiments we report, the continuous change in substrate or inhibitor concentration against time results only from the buffer composition reequilibrating spontaneously with the atmosphere of the glovebox and is fully uncoupled to the activity of the enzyme.

CO Inhibition Is Reversible and Fast. Inhibition of hydrogenase activity by CO is well-known to be reversible. However, in traditional experiments (solution assays), testing the reversibility usually involves exchanging the atmosphere above the sample and waiting for the solution to equilibrate: this takes several minutes. In contrast, PFV allows change in activity to be measured on much shorter time scales, and data such as those in Figure 4 show that CO binding occurs within the dead time for mixing (<0.5 s) and remains at equilibrium during the transient.

Since CO always equilibrates with the enzyme on the time scale of our experiments, we were able to determine dissociation constants with great simplicity by monitoring the recovery of activity while the added inhibitor vanishes from the cell. The values we determined are of the same order of magnitude as those measured at 25 °C with the enzyme from *D. gigas*:[42] $K_I(CO/H^+) = 8 \times 10^{-3}$ atm CO, $K_I^{app}(CO/H_2) = 2 \times 10^{-1}$ atm CO under 1 atm of H_2.

Assuming that CO inhibition of H_2 oxidation is competitive,[42,43] the apparent inhibition constant under saturating conditions is expected to be proportional to C_{H_2} (eq 6), as indeed observed in our experiments (Figure 5): at −160 mV, the inhibition constant measured under 1 atm of H_2 was 10 times greater than that measured under 0.1 atm of H_2. Taking into account the value of the Michaelis−Menten constant for H_2 oxidation, we determined the value of the affinity for CO of the Ni−SI state that is present under oxidizing conditions: $K_{SI} = 6.6 \times 10^{-4}$ atm CO ($\approx$0.65 μM).

Beyond the simplicity of the experimental method we propose (with respect to solution assays), we are provided with a unique way of looking at how the affinity for CO continuously changes as the driving force for the H^+/H_2 conversion is tuned (Figure 5). By repeating CO additions at different values of the electrode potential, while the enzyme evolved H_2 under an atmosphere of Ar (Figure 6), we have measured the continuous change in inhibition constant as a function of driving force (black squares in Figure 5): as the electrode potential is decreased, the apparent dissociation constant for CO increases continuously and remains greater than the intrinsic affinity for CO of the Ni−SI state. This dependence will now be interpreted in relation to the electrode-potential-dependent concentrations of the different states of the active site that are present during turnover, each having a specific affinity for CO.

Why Does CO Inhibit H_2 Evolution? At first sight, the increase in $K_I(CO/H^+)$ with decreasing electrode potential in Figure 5 may be simply interpreted in terms of a reduced form of the active site having a lower affinity for CO than the form present under oxidizing conditions. This would suggest that, at low electrode potential, inhibition of proton reduction results from binding of CO to the most reduced form of the active site, Ni−R. However, this is very unlikely to be the case for the following reasons.

(1) No state with CO bound to Ni−R has ever been observed in time-resolved experiments where the reduced enzyme was mixed with CO,[32,60] whereas the Ni−SI−CO species is stable enough to be isolated and crystallized.[40]

(2) Although the structure of Ni−R is still a matter of debate, the coordination sphere of the Ni ion is certainly complete, either because the Ni is bound to H_2 (this is favored from theoretical calculations[6]) or because a hydride bridges the metal ions. In either case, the active site could not accommodate an exogenous CO ligand in Ni−R, whereas there are spectroscopic and structural evidences for this to be the case in Ni−SI.[34−40] Similarly, binding of CO to the Ni−C state is difficult: it requires illumination under cryogenic conditions to remove the bridging hydride, and Ni−C−CO is obtained only in substoichiometric amounts.[60]

(3) If CO could bind to Ni−R, this would imply that CO and H_2 can bind simultaneously, and this would result in the inhibition by CO being mixed.[55] In contrast, available data[42,43] (including those reported above, regarding how the apparent inhibition constant changes with H_2 partial pressure) point to a competitive mechanism, whereby the substrate and the inhibitor cannot bind simultaneously.

Therefore, since CO binds only to the Ni−SI state, the fact that CO inhibits proton reduction reveals the presence of the oxidized, active form of the active site under reducing conditions. This can be explained by taking into account the finite rate of interfacial electron transfer: we have shown that the model developed previously[13] to analyze the catalytic wave shape for proton reduction could be extended to describe CO binding to Ni−SI (Supporting Information) and to derive an equation (S5) that could fit the dependence of the apparent inhibition constant on E (plain line in Figure 5). The reduction potentials of the active site determined from this fit were consistent with those measured by fitting the catalytic signals in Figure 1. In the fully reversible limit, that would be reached if there were no limitation by interfacial electron transfer, the dashed line in Figure 5 would be observed; in this case, the active site would equilibrate with the electrode potential,[49] and the disappearance of Ni−SI under reducing conditions would lead to an exponential increase in the apparent

(58) Schiller, M. R.; Holmes, L. D.; Boeker, E. A. *Biochim. Biophys. Acta* **1996**, *1297*, 17−27.
(59) Duggleby, R. G. *Methods* **2001**, *24*, 168−174.
(60) Happe, R. P.; Roseboom, W.; Albracht, S. P. J. *Eur. J. Biochem.* **1999**, *259*, 602−608.

inhibition constant, until, practically, CO no longer inhibits proton reduction. The limitation due to interfacial electron transfer makes the populations of each redox state under turnover conditions deviate from those under equilibrium conditions. This illustrates a case where the inhibition constant measured at a given potential under turnover conditions is not directly related to the affinity of the inhibitor for the redox state of the enzyme that is stable, at this potential, under equilibrium conditions.

Remarkably, the fact that CO also inhibits H_2 evolution in *solution* assays[42] shows that the redox mediators cannot keep the enzyme fully reduced either. This suggests again that, in traditional experiments, relatively slow intermolecular electron transfer may result in underestimating the intrinsic activities of NiFe hydrogenases.

Alternatively to slow interfacial and intermolecular electron transfers, another reason, not accounted for by our model, could also be responsible for the presence of some Ni−SI form of the active site under reducing conditions: the rate of reduction of the active site may level off as the electrode potential decreases (instead of increasing exponentially) because a chemical step that precedes the reduction of Ni−SI to a form that no longer binds CO is relatively slow. This slow step could be the protonation of Ni−SI after it has been reduced (a proton-transfer step was proposed to be rate limiting during H_2 evolution in ref 61) or the subsequent formation of the bridging hydride.

The reversibility of CO inhibition certainly makes sense from a physiological point of view, as CO is a common metabolite in anaerobic environments.[2] Keeping in mind the goal of using hydrogenase-based[17] or hydrogenase-like[62] catalysts in fuel cells, this also shows the superiority of Ni and Fe with respect to precious metals such as Pt and Pd, which are irreversibly poisoned by oxides.

Aerobic Inactivation Is Slow and First-Order in O_2. The fact that solution assays cannot be performed in the presence of oxygen had previously precluded the investigations of the kinetics of the aerobic inactivation,[63] despite the importance of such a process in the context of mechanistic studies, fuel cell technology, biological photoproduction of H_2 and metabolic regulation in microaerobic organisms.

Using PFV, the rate of H_2 oxidation by NiFe hydrogenase can be determined in the presence of O_2, and the rate of inactivation can be measured. This is done by (i) poising the potential of the electrode onto which hydrogenase is adsorbed at a high value (so that H_2 is catalytically oxidized and no direct reduction of O_2 occurs), (ii) continuously bubbling H_2 (or a mixture of H_2 and an inert gas) in the cell, and (iii) adding a small aliquot of O_2-saturated solution; the inactivation of the enzyme then results in a decrease in current. The plot of $d(\ln i)/dt$ (Figure 8B) provides a direct and intuitive visualization of how the inactivation slows down with time as the concentration of O_2 decreases. The good fit of the rate of inactivation to an exponential decay is an unambiguous evidence that, at least under the conditions of low O_2 concentration we used (<12 μM), the process is first-order in O_2.

To the best of our knowledge, this is the first measurement of the bimolecular rate constant for the inactivation of a NiFe hydrogenase with O_2. The attack of Df-hase by O_2, with a pseudo-first-order rate constant of $\approx 3 \times 10^4$ s^{-1} M^{-1} at 40 °C, is the slowest bimolecular process: the CO binding event is too fast to be resolved in our experiments (thus its rate constant must be at least an order of magnitude greater than that for reaction with O_2), and with a turnover for H_2 oxidation[12] greater than 1000 s^{-1} and a K_m value in the μM range, the value of the specificity constant k_{cat}/K_m must approach the diffusion limit.

The fact that the rate of aerobic inactivation does not depend on E at a given pH (Figure 9A) or on pH at a given E (panel B) shows that the steady-state fraction of Ni−SI state is independent of E in this range of electrode potential and that the attack by O_2 is not modified by a protonation equilibrium at the active site. A protonation step may still occur after the reaction with O_2, provided that it is not rate limiting.

Reaction with O_2 Produces a Mixture of Ni−A and N−B. From the cyclic voltammograms recorded under H_2 in Figure 1, it is clear that there exists a potential range within which the enzyme oxidizes H_2 without undergoing anaerobic inactivation (the formation of Ni−B would result in a characteristic decrease in current at high potential[15]). Accordingly, at pH 6, 40 °C, and even at a potential as high as −160 mV, the chronoamperometric data in Figure 4A show remarkably stable oxidative current over a large period of time. This is not the case at 190 mV and pH 7, where the activity decreases steadily (dotted line in Figure 8A) as a result of the anaerobic inactivation (increasing the pH and the electrode potential makes the oxidation to Ni−B more favorable[15]).

When the enzyme is inhibited by adding O_2, then reactivated at low electrode potential for 30 s and taken back to 190 mV, about half of the activity that was lost upon aerobic inactivation is recovered (Figure 7). Further reactivation could be observed by using much longer reductive poises (at pH 7, 40 °C, this required about 20 min). A similar observation was made with the enzyme from *A. vinosum* in ref 16. Since reactivation of Ni−B is virtually instantaneous at high temperature and low electrode potential,[15,16] this shows that the reaction of the active enzyme with O_2 results in the formation of a mixture of Ni−A (that is not reactivated during the short reducing poise) and Ni−B. Consistently, (i) the purification of the enzyme under aerobic conditions always leads to a mixture of Ni−A and Ni−B states,[9] and (ii) EPR data obtained with O_2-oxidized Av-hase exhibit line broadening for both the Ni−A and Ni−B states when $^{17}O_2$ is used instead of $^{16}O_2$ (ref 36). This shows that two distinct oxidation mechanisms, either aerobic or anaerobic, can lead to the formation of Ni−B from Ni−SI. Further experiments are in progress to identify the physical parameters and structural factors which determine the favorable formation of one particular inactive state under aerobic conditions.

Protection against O_2 by H_2 Is Not Complete. The structural and spectroscopic evidences[34−40] that exogenous CO binds the active site at the Ni are consistent with the earlier finding that CO and H_2 compete.[42,43] This is illustrated by our observation that, under saturating conditions, the apparent inhibition constant $K_I(CO/H_2)$ is proportional to the concentration of H_2. From a molecular point of view, this implies that H_2 must be released

(61) Bertrand, P.; Dole, F.; Asso, M.; Guigliarelli, B. *J. Biol. Inorg. Chem.* **2000**, *5*, 682−691.
(62) Evans, D. J.; Pickett, C. J. *Chem. Soc. Rev.* **2003**, *32*, 268−275.
(63) It is still possible to use solution kinetics to measure the extent of inactivation after incubation of the enzyme with oxygen (Erbes, D. L.; King, D.; Gibbs, M. *Plant Physiol.* **1979**, *63*, 1138−1142) or to follow the H−D exchange reaction in the presence of O_2 (Cournac, L.; Guedeney, G.; Peltier, G.; Vignais, P. M. *J. Bacteriol.* **2004**, *186*, 1737−1746).

before CO can bind, and this is in contrast with the mechanism of aerobic inactivation. Indeed, if O_2 were binding only to the H_2-free form of the active site, like CO does, the rate of inactivation would be proportional to $1/C_{H_2}$ under saturating conditions.[55] That this is not the case is obvious from our results: the bimolecular rate of reaction with O_2 is decreased only by a factor 2.5 when the H_2 pressure is increased from 0.1 to 1 atm (Figure 8). This implies that H_2 needs not be released before O_2 can bind to the active site, although its presence slows down slightly the inactivation: in other words, the attack by O_2 is not specific to the Ni−SI state.

Concluding Remark

Heterodimetallic NiFe model compounds relevant to the active site of hydrogenases are much more difficult to obtain that their di-iron counterparts, and a functional NiFe system has yet to be synthesized.[62] In this respect, the possibility to use genetic engineering to study the fully active, biological system[4,9,33,64] is a unique and exciting strategy to determine how the chemical environment of the bimetallic cluster affects its catalytic properties, including its sensibility to oxygen. In the near future, the methods presented in this paper will be essential to discriminate between active site mutants on the basis of their resistance to aerobic inactivation.

Acknowledgment. We thank Athel Cornish-Bowden and Claude Hatchikian (Unité de Bioénergétique et Ingénierie des Protéines, Marseille) and Victor M. Fernandez and Antonio De Lacey (Departamento de Biocatálisis, Instituto de Catálisis, Madrid) for fruitful discussions. This work was funded by the CNRS, the "Université de Provence," the "Ville de Marseille," and by the Grant G5RD-CT-2002-00750 from the European Commission Competitive and Sustainable Growth Program. Marc Rousset is "Laboratoire de Recherche Conventionné avec le CEA" No25V.

Supporting Information Available: Figures S1 and S2 (H_2 and CO inhibition of H_2 evolution, respectively) and derivation of equation S5, which is used to fit the dependence of $K_I(CO/H^+)$ on E. This material is available free of charge via the Internet at http://pubs.acs.org.

JA046548D

(64) De Lacey, A. L.; Fernandez, V. M.; Rousset, M.; Cavazza, C.; Hatchikian, E. C. *J. Biol. Inorg. Chem.* **2003**, *8*, 129−134.